Phase Separation of Poly(*N*-isopropylacrylamide) in Mixtures of Water and Methanol: A Spectroscopic Study of the Phase-Transition Process with a Polymer Tagged with a Fluorescent Dye and a Spin Label

by **M. Francesca Ottaviani**

Institute of Chemical Sciences, University of Urbino, piazza Rinascimento 6, I-61029 Urbino (e-mail: ottaviani@uniurb.it)

and **Françoise M. Winnik**

Université de Montréal, Faculté de Pharmacie et Département de Chimie, C.P. 6128, Succursale Centre Ville, Montréal QC, H3C3J7 Canada (e-mail: francoise.winnik@UMontreal.CA)

and **Stefan H. Bossmann**

University of Karlsruhe, Engler-Bunte-Ring 1, D-76128 Karlsruhe (e-mail: ie61@mv70.rz.uni-karlsruhe.de)

and **Nicholas J. Turro**

Department of Chemistry, Columbia University, 3000 Broadway, Mail Code 3119, New York, NY 10027, USA (e-mail: turro@chem.columbia.edu)

Dedicated to Prof. Dr. *André M. Braun* on the occasion of his 60th birthday

The thermoreversible phase transition of poly(*N*-isopropylacrylamide) randomly labeled with a spin label, 4-amino-2,2′,6,6′-tetramethylpiperidine 1-oxide (TEMPO), and a fluorescent dye, 4-(pyren-1-yl)butyl (PNIPAM-Py-T), in different H_2O/MeOH mixtures was studied by turbidimetry, continuous-wave electron paramagnetic resonance spectroscopy (CW-EPR), and fluorescence spectroscopy. The macroscopic phase diagram of PNIPAM-Py-T in H_2O/MeOH measured by turbidimetry was identical to those of poly(*N*-isopropylacrylamide) (PNIPAM) and of TEMPO-labeled PNIPAM (PNIPAM-T) in H_2O/MeOH mixtures. However, distinct differences among the three polymers were detected in their solvent-dependent EPR and fluorescence-spectroscopic properties. The EPR spectra were analyzed in terms of the isotropic hyperfine coupling constants, which monitor the variation in environmental polarity of the radical labels occurring for the conformational transitions of the polymer as a function of temperature, as well as the correlation time for reorientation motion, the increase of which is indicative of the increased viscosity of the radical environment and interactions occurring between the radical and other surface groups of the precipitated polymer, if compared to the soluble polymer. The fluorescence of Py in PNIPAM-Py-T displayed contributions from isolated excited pyrenes (monomer emission) and from preformed pyrene ground-state aggregates (excimer emission). The quantum efficiencies of monomer and excimer emission were monitored as a function of solvent composition. By the two experimental approaches, we demonstrate the profound influence of the PNIPAM-attached pyrene units in increasing the hydrophobicity of the nanodomains formed upon heat-induced precipitation of PNIPAM-Py-T.

Introduction. – The fast-growing progress in nanotechnology and life sciences have created an urgent need for novel 'intelligent' polymer hydrogels, which might allow the synthesis and application of vital nanocomponents. Nanocomponents have substantial advantages over conventional polymeric particles. Their reduced size permits a faster response to environmental changes [1]. Furthermore, polymer nanoparticles can be

used as building blocks in molecular nano-architecture of the future and for the tailoring of biocomposite materials [2]. Any successful application of such intelligent hydrogels will be highly dependent on their physical properties. The controlled formation of strongly hydrophobic nanodomains is of particular importance. In this area, the synthesis of uncharged polymer latex nanoparticles possessing accessible π-bonds has been reported recently using poly(*N*-isopropylacrylamide) as a template [3]. A possible fine-tuning of the hydrophobicity of these polymer nanodomains would be considered as a real break-through in materials science. We have devoted our efforts to reach this goal during the last decade and present here a fundamental study by spectroscopy of the nano-architecture on phase-separated poly(*N*-isopropylacrylamide) derivatives.

The temperature-induced phase transition of poly(*N*-isopropylacrylamide) (PNIPAM; *Fig. 1*) provides the ideal tool to investigate the physical properties of the formed thermoreversible hydrogels in the presence of H_2O and in aqueous solvent mixtures [4]. Aqueous solutions of PNIPAM show a reversible temperature-induced phase separation. When an aqueous solution of PNIPAM is heated past *ca.* 31° (the cloud-point or lower critical solution temperature, LCST), the polymer precipitates from solution leading to a two-phase system. The solubility of PNIPAM in cold H_2O can be attributed to the ability of the macromolecule to form H-bonds to H_2O molecules *via* the amide functional groups. At the same time, the apolar i-Pr substituents of the *N*-isopropylamido side chains induce a considerable ordering of H_2O or the aqueous solvent. Such polymer-H_2O interactions were inferred from experimental results based primarily on FT-IR spectroscopy [5][6]. This ordering of H_2O causes large negative contributions to both the enthalpy of mixing, ΔH_M, and the entropy of mixing, ΔS_M. When the temperature reaches the LCST, the entropy contribution to the free energy of mixing, ΔG_M, will overcome the negative enthalpy of solution. Thus, the free energy of mixing takes a positive value, and the phase separation of the polymer solution begins [7]. The macroscopic phase separation can be explained by a mechanistic paradigm, built upon a set of data obtained from various experimental techniques, such as microcalorimetry [8], dynamic and static light-scattering [9], fluorescence [10], and EPR and NMR spectroscopy [11]. Each technique has its limitations and is sensitive only to certain distance scales and time windows. Therefore, for a specific study it is mandatory to chose spectroscopic methods that are complementary to each other. In studying poly(*N*-isopropylacrylamide) featuring chemically attached 2,2′,6,6′-tetramethylpiperidine 1-oxide (TEMPO) and pyrene groups, we employed EPR spectroscopy and fluorescence studies in order to probe by two spectroscopic tools the hydrophobicity of the PNIPAM-Py-T phase that precipitates from solution above its cloud point. Both methods work in approximately the same time window (EPR $10^{-11}-10^{-6}$ s; fluorescence $10^{-10}-10^{-7}$ s) and are very sensitive to changes in the polarity and microviscosity of the local environment of the respective probes, TEMPO and pyrene [11].

We have studied previously the temperature-induced phase separation in mixed aqueous solutions of a TEMPO-labeled PNIPAM [12]. From the CW-EPR results, we proposed a mechanism involving the extrusion of H_2O from the polymer chain and preferential adsorption of MeOH during the precipitation process, together with increasing hydrophobically driven attraction of individual polymer segments. The analysis of the EPR hyperfine coupling ($\langle A_N \rangle$) of the three-line TEMPO spectrum

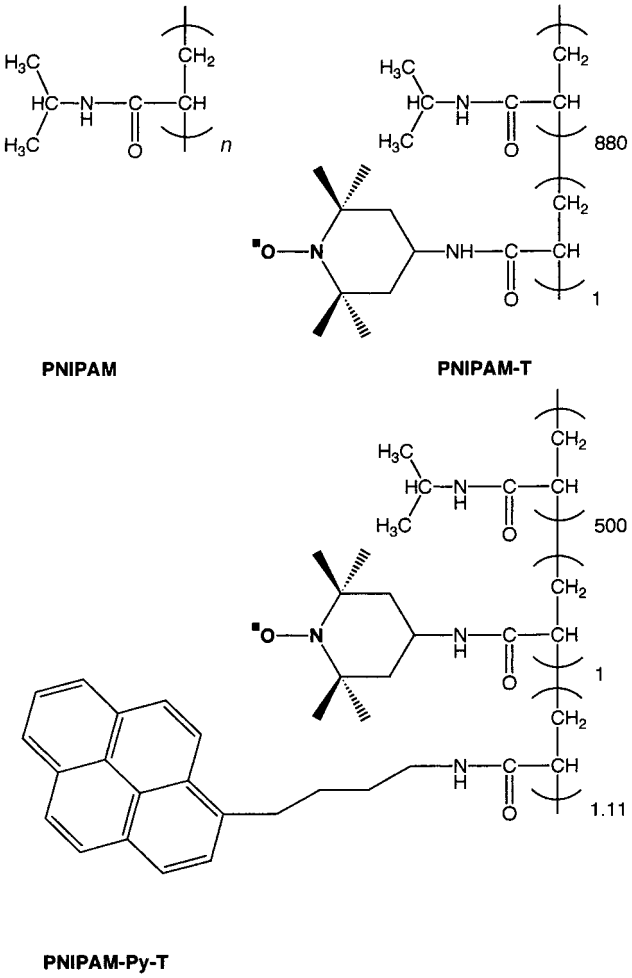

Fig. 1. *Structures of PNIPAM, PNIPAM-T, and PNIPAM-Py-T*

indicated that, above the LCST, PNIPAM forms strongly hydrophobic domains in H_2O/MeOH mixtures. The size of the individual nanodomains formed by the collapse of individual PNIPAM chains was estimated to be in the range of 2–20 nm from transmission electron microscopy [13]. The PNIPAM precipitate is then formed by the clustering of these individual PNIPAM nanostructues [12], a mechanistic hypothesis supported by a recent study by dynamic light scattering of extremely dilute PNIPAM solutions in H_2O/MeOH mixtures [14]. If conditions can be found where the size distribution of such PNIPAM nanodomains is very narrow, then the hydrophobic nanodomains embedded within an aqueous environment would present themselves as very promising nanoreactors. This approach could lead to a real breakthrough in the design of hydrogel-reaction systems, if the hydrophobicity of these nanodomains could be triggered by hydrophobic labels linked to the PNIPAM chain in very low density.

Experimental. – *Materials.* All chemicals were purchased from *Aldrich Chemical Co.*, unless otherwise noted. *N*-Isopropylacrylamide was bought from *Eastman Kodak Chemicals*. 4-Amino-2,2′,6,6′-tetramethylpiperidine 1-oxide (4-amino-TEMO) was used as received. H_2O was deionized with a *Millipore Milli-Q* water purification system. HPLC-Grade solvents were used for the composition of ternary systems (PNIPAM/H_2O/solvent). For synthesis, reagent-grade solvents were used without further purification, except for THF, which was distilled from Na/benzophenone under N_2 prior to use. The reactive polymer, *N*-isopropylacrylamide/*N*-(acryloxy)succinimide copolymer (PNIPAM-NASI), was synthesized by free-radical copolymerization of *N*-isopropylacrylamide and *N*-(acryloxy)succinimide in *t*-BuOH, as described in [10].

*Synthesis of Poly(*N*-isopropylacrylamide/*N*-(2,2′,6,6′-tetramethyl-1-oxidopiperidin-4-yl)acrylamide/[4-(pyren-1-yl)butyl]acrylamide) Copolymer* (PNIPAM-Py-T; *Scheme 1*). A soln. of PNIPAM-NASI [10] (1.0 g) and 4-amino-2,2′,6,6′-tetramethylpiperidine 1-oxide (4-amino-TEMPO; 6.0 mg, 3.5×10^{-5} mol) in anh. THF (30 ml) was stirred at 298 K in the dark under N_2 for 17 h. First, a soln. of [4-(pyren-1-yl)butyl]ammonium hydrochloride (5.0 mg, 1.54×10^{-5} mol) in THF (2 ml) and then Et_3N (0.2 ml) were added [10]. The mixture was stirred at 298 K for 24 h. Then, (i-Pr)NH_2 (0.1 ml) was added to the mixture to quench unreacted *N*-oxidosuccinimido groups. Stirring was continued for another 3 h. The crude polymer was isolated by precipitation in hexane and was further purified by precipitation of dioxane solns. in Et_2O. The precipitate was dried in high vacuum at 40°, dissolved in H_2O, and isolated by freeze-drying. The polymer was characterized by GPC, which confirmed the absence of low-molecular-weight impurities. As expected, the chemical transformations did not alter the (broad) molecular-weight distribution of the copolymers. The amount of chemically attached pyrene was determined using UV absorption spectroscopy ($\lambda_{max} = 265, 275, 312, 326$, and 342 nm) using 4-(pyren-1-yl)butylamine hydrochloride ($\lambda_{max} = 342$ nm, $\varepsilon = 32800\,M^{-1}\,cm^{-1}$) as reference compound [15]. The content of attached TEMPO was determined by comparing the EPR signal of 4-amino-TEMPO/PNIPAM mixtures, dissolved in MeOH at 293 K, with that of PNIPAM-Py-T under the same experimental conditions. Viscosity-averaged molecular weights were calculated from the intrinsic viscosity $[\eta] = 9.59 \times 10^{-3}\,M_v^{0.65}\,cm^3 \cdot g^{-1}$ [16]. Pyrene content: 1.9×10^{-5} mol · g^{-1}, TEMPO content 9.8×10^{-6} mol · g^{-1} or 1 pyrene/400 NIPAM units and 1 TEMPO/450 NIPAM units.

Scheme 1. *Preparation of TEMPO- and Pyrene-Labeled Poly*(N-*isopropylacrylamide)*

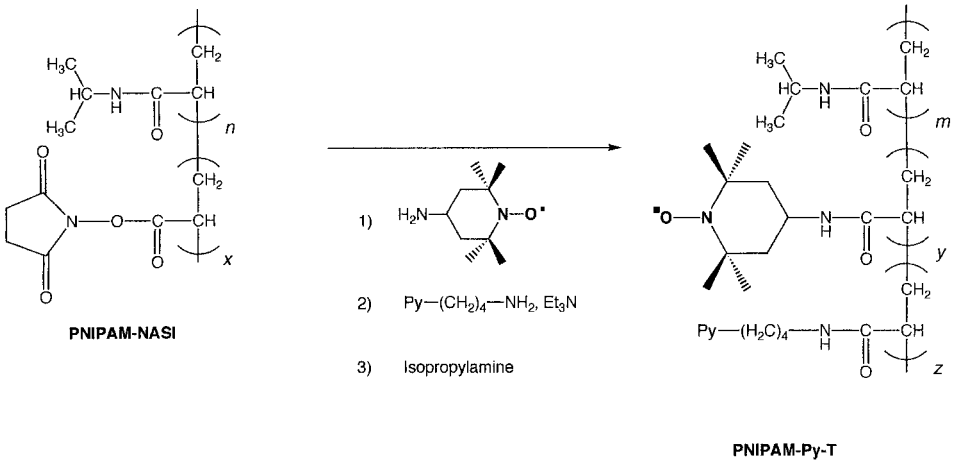

The chemical composition as well as the physical properties of the synthesized PNIPAM-Py-T copolymer are summarized in the *Table*.

Instrumentation. UV Spectra were recorded employing a *Varian UV-VIS-NIR Cary-5* spectrophotometer. Soln. viscosities were measured at 30° with a *Viscotek Model 100* differential viscometer (THF, polymer concentration 75 ± 3 mg · kg^{-1}). A *Waters WISP 700* system equipped with a *Waters RI 410* refractive-index detector was employed for gel permeation chromatography (GPC). Four ultrastyragel columns (10000, 5000, 500, and 100 Å) were used. The eluent (THF) was used at a flow rate of 0.8 ml · min^{-1}. Cloud points were

determined by spectrophotometric detection of changes in turbidity of solns. ($1.0\ g \cdot l^{-1}$) heated at a constant rate ($0.2^\circ\ min^{-1}$) in a magnetically stirred UV cell, as described in [10]. EPR Spectra were recorded with a *Bruker ESP 300* spectrometer with an *ESP 1600* data-analysis software. Temp. control ($T \pm 1^\circ$) was achieved using a *Bruker ER 4111T* variable-temp. unit. Steady-state fluorescence spectra were recorded with *SPEX* fluorescence spectrometers (*DM1B* or *DM212*) equipped with a *DM2000F* data-analysis program.

Table. *Physical Properties of the Polymers*

Polymer	$[\eta]$[a]) $[cm^3\ g^{-1}]$	$M_{viscosity}$[b])	M_n[c])	M_w[c])	LCST $[1.0\ g\ l^{-1}]$	[Py] $[mol\ g^{-1}]$	Attached TEMPO $[mol\ g^{-1}]$
PNIPAM	72 ± 1	0.92×10^6	55000	120000	32.5		
PNIPAM-T	151 ± 3	2.9×10^6	90000	340000	32.2		1.0×10^{-5}
PNIPAM-Py	141 ± 3	2.6×10^6	87000	340000	32.4	4.2×10^{-5}	
PNIPAM-Py-T	132 ± 3	2.3×10^6	85800	360000	31.2	1.9×10^{-5}	0.88×10^{-5}

[a]) From THF solutions. [b]) From $[\eta] = 9.59 \times 10^{-3}$ Mv (see [16]). [c]) GPC in THF, calibrated employing polystyrene standards.

Analysis of the EPR Spectra. The analysis of the recorded EPR signals was performed by the procedure reported by *Schneider* and *Freed* [17]. This procedure is particularly well-suited for the analysis of EPR signals originating from (chemically attached) nitroxides in slow motion conditions, *i.e.*, correlation times for rotational diffusion between 5×10^{-7} and 1×10^{-9} s. The procedure for obtaining the best fits was as follows: *1*) The input magnetic parameters for the *g* and *A* tensor components, the *Zeeman* and hyperfine interactions, respectively, were evaluated by computing the spectra in the slowest motion (at 77 K). The following parameters were obtained for the different solvents:

H_2O: $g_{xx} = 2.0087$, $g_{yy} = 2.0064$, $g_{zz} = 2.0038$; $A_{xx} = 6$ [G], $A_{yy} = 7.5$ [G], $A_{zz} = 36.5$ [G];
MeOH: $g_{xx} = 2.0087$, $g_{yy} = 2.0064$, $g_{zz} = 2.0038$; $A_{xx} = 6$ [G], $A_{yy} = 7.5$ [G], $A_{zz} = 34.5$ [G];
THF: $g_{xx} = 2.0087$, $g_{yy} = 2.0064$, $g_{zz} = 2.0038$; $A_{xx} = 6$ [G], $A_{yy} = 6.0$ [G], $A_{zz} = 33.0$ [G].

The parallel and perpendicular components of the rotational diffusional tensor, $D_\parallel$ and $D_\perp$, respectively, were obtained from the fitting between the experimental and computed spectra assuming *Brownian* motion. The simulations included a tilt angle of the rotational diffusional axes with respect to the magnetic molecular axes and an anisotropy of motion indicated by $N = D_\parallel/D_\perp$. The anisotropy parameter was calculated for each solvent as $N = 4$ in H_2O, $N = 15$ in MeOH, and $N = 50$ in THF.

In cases where more than one signal contributed to the EPR spectra, each signal was computed separately and added in a ratio appropriate to simulate the experimental spectrum. A subtraction-addition procedure was performed in order to identify the spectrum line shapes. The accuracies in the determination of rotational correlation times were $\pm 10\%$ and ± 0.05 G in the determination of hyperfine coupling constants.

Preparation of Samples for EPR Analysis. Solns. of PNIPAM-Py-T for EPR analysis were prepared by dissolving $4.0\ g \cdot l^{-1}$ of the copolymer in either H_2O or MeOH. The solns. were allowed to equilibrate for at least 24 h and then stored in a refrigerator. The solns. were degassed by a 20 min purge using Ar (4.5). The conditions for the most effective degassing were adjusted by a method based on the determination of the biacetyl fluorescence to phosphorescence emission [18].

Fluorescence Measurements. Steady-state and lifetime measurements were performed with an excitation wavelength of 332 nm. The emission was monitored at 380 nm (monomer lifetimes) or 480 nm (excimer lifetimes) unless otherwise specified. In the steady-state experiments, excitation and emission slit widths were set at 6 and 1 nm, respectively. The concentrations of the polymer soln. were $2.0\ g \cdot l^{-1}$. They were prepared by mixing and following dilution of a previously prepared polymer stock solns. of $20\ g \cdot l^{-1}$ and kept at r.t. for 12 h prior to analysis. All solns. were degassed by freeze-pump and thaw cycles or by bubbling with Ar for at least 20 min. Measurements carried out with samples degassed by the two different techniques yielded identical results within the error limit of $\pm 2\%$. Quantum yields were calculated by integration of peak areas of corrected spectra in wavenumber units, using as standard quinine sulfate in 1N H_2SO_4 ($\phi = 0.546$, $\lambda_{exc} = 328$ nm, $T = 298$ K) [19]. *Beer*'s law corrections were applied for optical density changes at the excitation wavelength. Corrections were made to account for differences in the refractive indexes as well. The excimer-to-monomer emission ratio

was calculated by taking the ratio of the emission intensity (peak height) at 480 nm to the half-sum of the emission intensities at 378 and 396 nm.

Results and Discussion. – The synthesis of the pyrene- and TEMPO-labeled PNIPAM copolymer was performed by reacting a copolymer of *N*-isopropylacrylamide and *N*-(acryloxy)succinimide (PNIPAM-NASI), first with 4-amino-2,2′,6,6′-tetramethylpiperidine 1-oxide (4-amino-TEMPO) and then with 4-[(pyren-1-yl)butyl]ammonium hydrochloride. Finally, the unreacted active ester functions were reacted with (i-Pr)NH_2 in order to avoid any possible formation of carboxylic acid groups by hydrolysis of residual NASI groups on the TEMPO- and pyrene-labeled copolymer. This synthetic route, similar to that employed to prepare PNIPAM [10], PNIPAM-Py [10], and PNIPAM-T [12], leads to polymers of high molecular weight and broad polydispersity.

1. *Phase-Diagrams of PNIPAM, PNIPAM-T, and PNIPAM-Py-T in H_2O/MeOH Mixtures.* In *Fig. 2*, the phase diagrams of the three employed PNIPAM-(co)-polymers are shown. All LCST's were determined employing the cloud-point method. The differences in the LCSTs are minor. In H_2O, the LCSTs of PNIPAM and PNIPAM-T are $32 \pm 0.5°$, whereas PNIPAM-Py-T has a LCST of $31.2 \pm 0.5°$. The LCST minima of

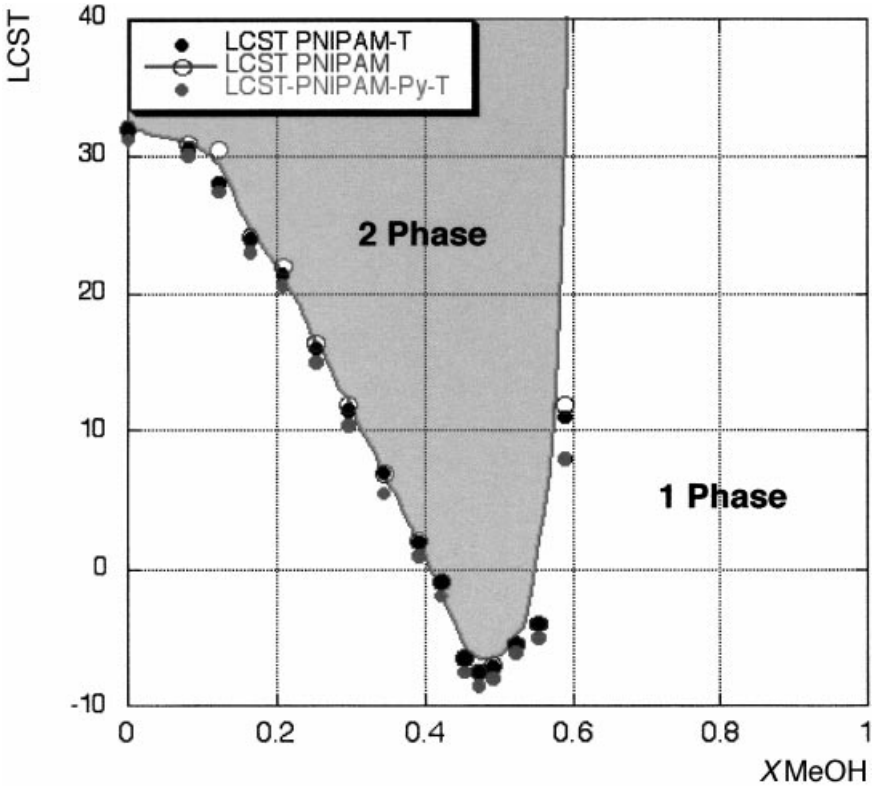

Fig. 2. *Ternary phase diagrams of PNIPAM, PNIPAM-T, and PNIPAM-Py-T in H_2O/MeOH*

all three PNIPAM polymers were found at 50 vol-% of MeOH ($X=0.471$); PNIPAM and PNIPAM-T at $-7.5\pm0.5^\circ$. PNIPAM-Py-T at $-8.5\pm0.5^\circ$. The phase diagrams of the three investigated polymers showed the typical 'clear point' (point of spontaneous demixing) at 64.4 ± 0.25 vol-% of MeOH ($X=0.589$). In conclusion, the three phase diagrams almost superimposed, when observed by using the cloud-point method, which is only concerned with the temperatures of the appearance of the turbidity of the polymer/solvent solutions. Therefore, EPR and fluorescence spectroscopy were employed to further elucidate any differences in the physical properties of the investigated (co)polymers.

2. *EPR Spectroscopy.* The EPR spectra of TEMPO, chemically attached to PNIPAM, exhibit the typical three-line pattern due to the coupling of the electronic spin of the nitroxide radical with the nuclear spin ($I=1$) of the ^{14}N nucleus. The EPR line shapes recorded here are analyzed by taking into account mobility and structural parameters to solve the spin *Hamiltonian* and the relaxation matrix. The following parameters were extracted from the spectral analysis: the line-widths and the correlation times for rotational motion. The correlation times for motion provide valuable information of the local mobility of the polymer-attached spin label. In the case of PNIPAM-Py-T and PNIPAM-T in MeOH or THF, the motion characteristic of the linked spin label is highly anisotropic (*Fig. 3*). In such a particular case, it is possible to determine the parallel and perpendicular components of the correlation times for the motion of the label.

PNIPAM-Py-T dissolved in MeOH ($T=25^\circ$) possesses only one EPR component due to labels in fast motion ($\tau_c=7\times10^{-10}$ s), but the increase of τ_c with respect to free nitroxides in solution (*ca.* 10^{-11} s) indicates that TEMPO is indeed bound to the polymer backbone. Spin-labeled low-molecular-weight components are clearly absent.

The analysis of the spectra shown in *Fig. 3* takes into account the tilt of the main rotational axis toward the N–O direction ($z'=x$), which indicates a rather fast mobility of the probe along the N–O direction ($\tau_c=9.9\times10^{-11}$ s for MeOH; $\beta_c=9.5\times10^{-11}$ s for THF) and a remarkably slower motion ($\tau_c=5\times10^{-9}$ s for MeOH; $\tau_c=4.7\times10^{-9}$ s for THF) in the perpendicular direction. This is a clear indication of the restriction of motion experienced by the chemically attached nitroxide function. Note that the observed decrease of motion along the direction perpendicular to the N–O direction is most likely not only caused by the chemical attachment of TEMPO to the PNIPAM-polymer chain, but it can be also regarded as a strong experimental indication of the binding of solvent molecules to the polymer chain [15]. In fast conditions ($\tau_c<1\times10^{-9}$ s), the anisotropies are averaged to zero, and the isotropic hyperfine coupling constant $\langle A_N\rangle$ offers the opportunity to measure the local polarity in the molecular environment of the TEMPO-spin probe.

The analysis of the EPR spectrum of PNIPAM-Py-T in H_2O ($T=25^\circ$) revealed the presence of two components (*Fig. 3*). It was computed as the sum of two signals and the different percent contribution of each spectral component, adopting the following fitting procedure. First, a subtraction-addition routine was performed to identify each component. In the second step, magnetic and mobility parameters were computed by the spectral simulation method by *Schneider* and *Freed* [17], assuming *Lorentzian* line-shape of the signal, and isotropic motion of the spin label. The magnetic parameters of

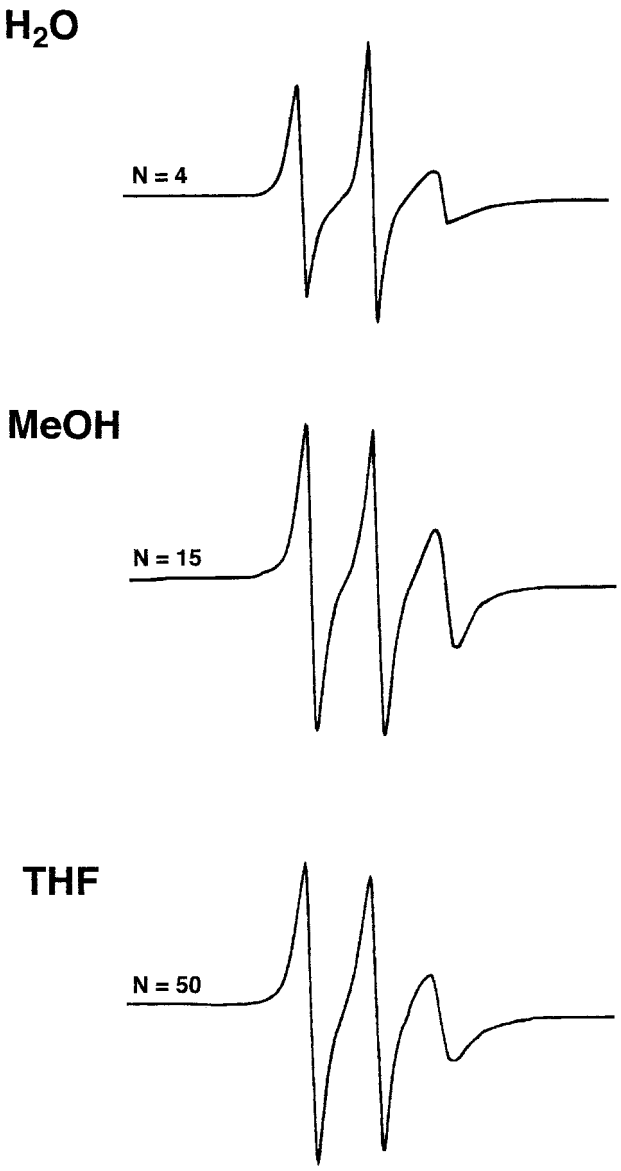

Fig. 3. *EPR Spectra of pyrene- and TEMPO-labeled poly(*N-*isopropylacrylamide) (PNIPAM-Py-T) in H_2O, MeOH, and THF* ($T = 25°$, polymer concentration 4 g·l^{-1})

4-amino-TEMPO in H_2O [11] were employed[1]). Based on these assumptions, the EPR signals of PNIPAM-Py-T in H_2O ($T = 25°$) were calculated to A: $\tau_c = 2 \times 10^{-10}$ s (12%) and B: $\tau_c = 1.5 \times 10^{-9}$ s (88%). We rationalize the occurrence of a minor and a major

[1]) When the same procedure was applied in different solvents, the magnetic parameters for the appropriate solvent (or solvent mixture) were used.

component by the *syn-anti*-equilibrium of chemically attached 4-amino-TEMPO, which is an intrinsic feature of the amide bond, used to connect the spin probe with the polymer backbone. Calorimetric measurements during the process of LCST indicated that H_2O is strongly bound to the PNIPAM polymer below the LCST *via* H-bonding [5][6][11][20]. When the LCST phenomenon occurs upon heating, it becomes almost completely extruded during the precipitation process. This process is endothermic [8]. The polymer-bound H_2O is able to slow down the exchange rate between those conformers sufficiently that they become discernible in the EPR timescale. *Scheme 2* indicates the mechanistic hypothesis.

In our previous work, we have studied the mechanism of the temperature-reversible LCST phase transitions of PNIPAM-T in ternary solvent mixtures [10], and of PNIPAM-Py-T in H_2O [12]. Characteristic changes occurred in the EPR spectra as a function of temperature, as the solutions were heated through their LCSTs. Below the LCSTs, two components were prevailing: a very fast minor component A: $\tau_c = 1-3-10^{-10}$ s (see above) and a major component B: $\tau_c = 1-4\times10^{-9}$ s, which was distinctly lower in mobility. Most significant was the sudden growing of a new component C at the expense of component B during heating. Component C was characterized in all the investigated cases by a much longer correlation time ($\tau_c = 6-9\times10^{-9}$ s). However, component A was not much affected during this transition. *Fig. 4,a*, shows a typical superposition of the spectral components A, B, and C during a LCST transition. The equilibria between the different spectral components below and above the LCST are indicated in *Fig. 4,b*.

Analysis of the Hyperfine Coupling Constants $\langle A_N \rangle$. The analysis of the isotropic hyperfine coupling constant $\langle A_N \rangle$ provided very valuable information about the polarity of the nano-environment in the direct proximity of the chemically attached TEMPO spin probes. The dependence of $\langle A_N \rangle$ on the polarity arises from the delocalization of the radical electron between the N- and the O-atom [21]. Thus, a higher $\langle A_N \rangle$ value is observed in a polar environment that delocalizes the electron density towards the O-atom of NO ($\langle A_N \rangle$ in H_2O: 17.1 [G]). In nonpolar solvents, this

Scheme 2. syn-anti-*Equilibrium of Chemically Attached 4-Amino-TEMPO with Respect to the PNIPAM Polymer Backbone*[1])

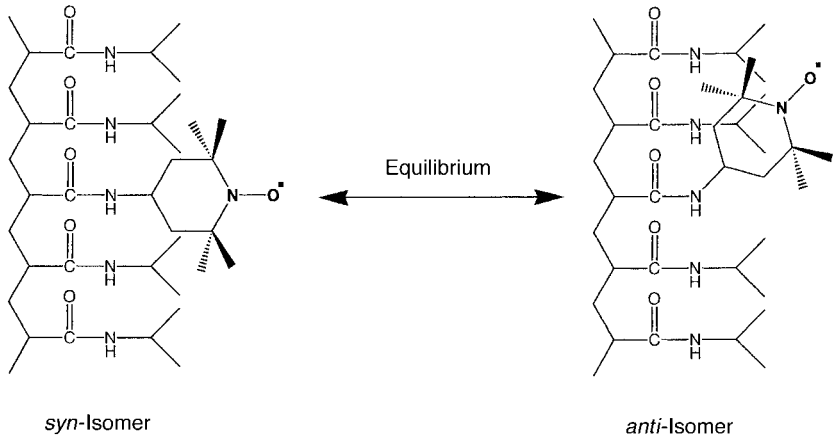

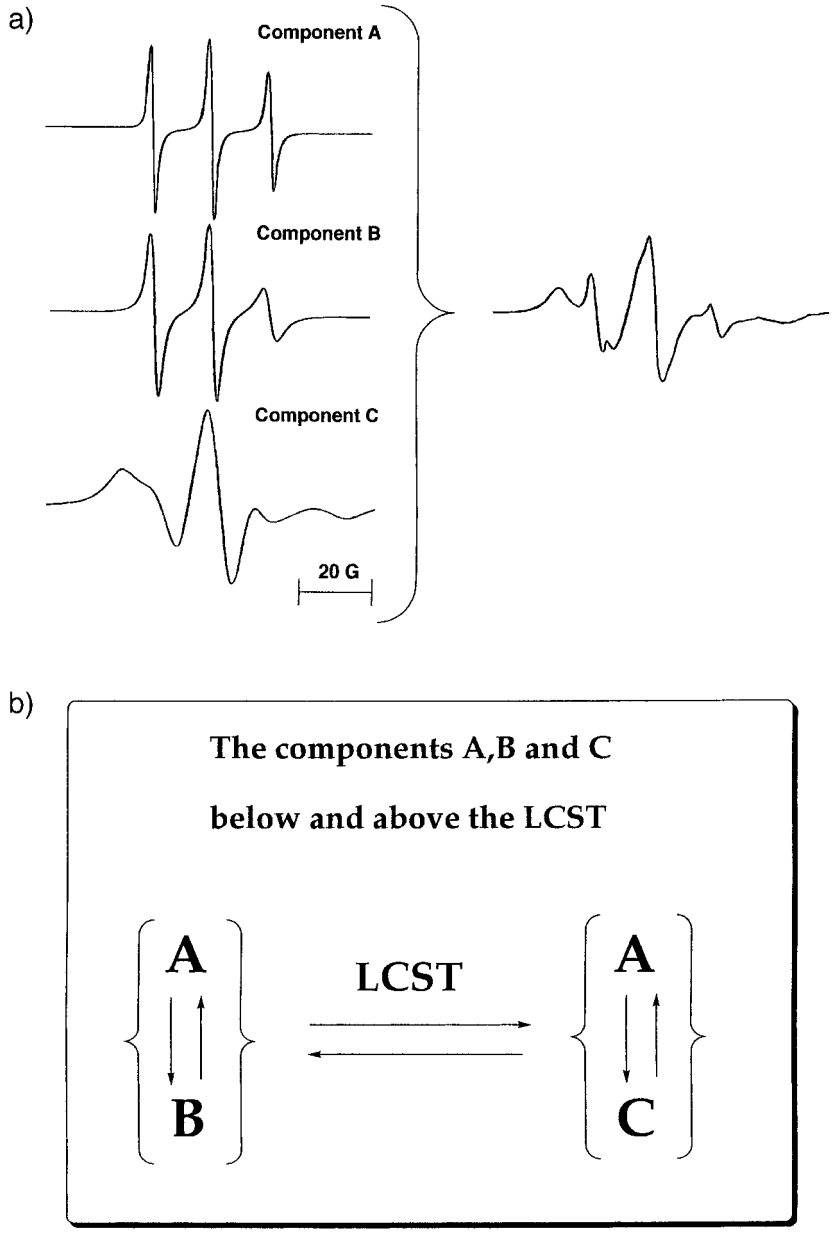

Fig. 4. a) *Superposition of the spectral components A, B, and C.* b) *Equilibria between the different spectral components below and above the LCST.*

effect is not observed, and, therefore, the electron density is mainly centered on the N-atom, resulting in a smaller hyperfine coupling constant ($\langle A_N \rangle$ in THF: 15.65 [G]). In *Fig. 5*, the measured isotropic hyperfine coupling constants of 4-amino-TEMPO in four

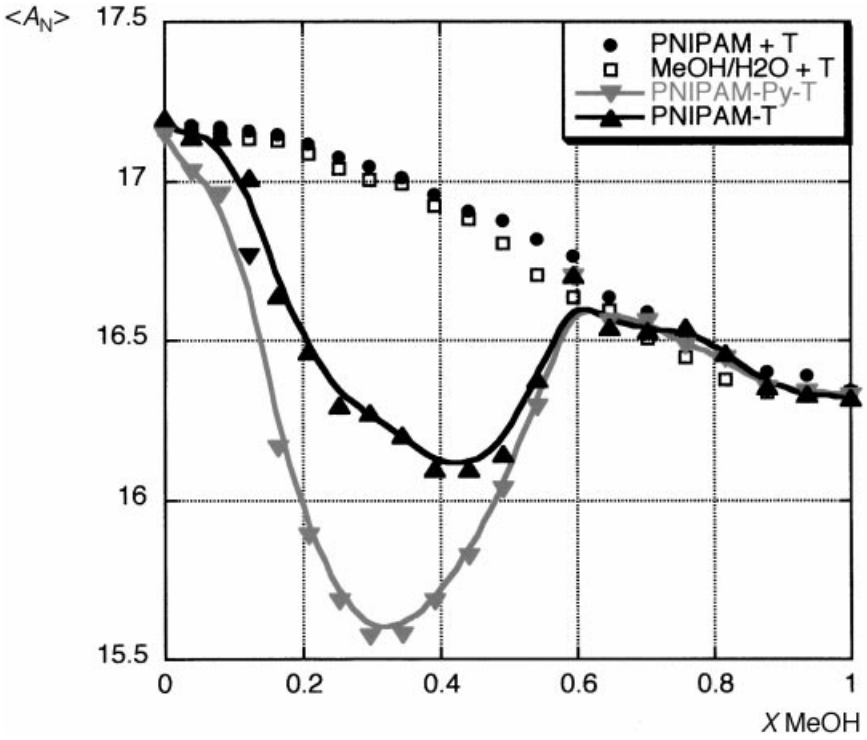

Fig. 5. *Isotropic hyperfine coupling constants of 4-amino-TEMPO measured at 20° in H_2O/MeOH, in H_2O/MeOH in the presence of PNIPAM* (4.0 g·l^{-1}), *PNIPAM-T* (4.0 g·l^{-1}) *in H_2O/MeOH, and PNIPAM-Py-T* (4.0 g·l^{-1}) *in H_2O/MeOH*

different chemical systems along the *x*-axis (*X* MeOH) at $T = 20°$ are compared: whereas 4-amino-TEMPO in H_2O/MeOH and 4-amino-TEMPO in H_2O/MeOH in the presence of 4.0 g·l^{-1} PNIPAM show a slightly S-shaped decrease from 17.1 [G] (pure H_2O) to 16.3 [G] (pure MeOH), no local minima in $\langle A_N \rangle$ were detected!

In nonpolar solvents, this complexation is not observed, and, therefore, the electron density is weighted more heavily on the N-atom, resulting in a smaller hyperfine coupling constant ($\langle A_N \rangle$ in THF: 15.65 [G]). In *Fig. 5*, the measured isotropic hyperfine coupling constants of 4-amino-TEMPO in four different chemical systems along the *x*-axis (*X* MeOH) at $T = 20°$ are compared: whereas 4-amino-TEMPO in H_2O/MeOH and 4-amino-TEMPO in H_2O/MeOH in the presence of 4.0 g·l^{-1} PNIPAM show a slightly S-shaped decrease from 17.1 [G] (pure H_2O) to 16.3 [G] (pure MeOH), no local minima in $\langle A_N \rangle$ were detected! In sharp contrast, EPR measurements employing 4-amino-TEMPO-labeled PNIPAM (PNIPAM-T) revealed a strong decrease of $\langle A_N \rangle$ in the region, where the LCST of the polymer is observed.

PNIPAM-Py-T shows a decrease in the $\langle A_N \rangle$ minimum, which is much steeper than previously observed with PNIPAM-T. Since the structures of PNIPAM-Py-T and PNIPAM-T differ only in the presence/absence of the attached hydrophobic aromatic hydrocarbon, we concluded that pyrene is the responsible factor for the observed

differences in $\langle A_N \rangle$ for both spin-labeled polymers (see below). Photophysical investigations of PNIPAM-Py/200 revealed the formation of so-called preformed pyrene excimers, which are formed when the polymer is dissolved (one-phase region of the ternary phase diagram) [10]. The driving force is the hydrophobic (Π)-stacking of polymer-bound pyrene units. This influence is clearly discernible from the data shown in *Fig. 5*. When polymer-attached pyrene is present (PNIPAM-Py/400-T/450), the decrease of $\langle A_N \rangle$ starts at 17.1 [G] in H_2O. When $X = 0.2$ is reached, we enter the LCST domain of both PNIPAM-T and PNIPAM-Py-T. However, a striking difference in $\langle A_N \rangle$ of both polymers is apparent: when employing PNIPAM-T, $\langle A_N \rangle$ at ($X = 0.2$) is 16.5 [G], whereas, when using PNIPAM-Py-T, a much lower value of $\langle A_N \rangle = 15.9$ [G] was observed, indicating that the hydrophobicity of that particular PNIPAM-Py-T precipitate is strongly increased compared to PNIPAM-T. The same trend continues with increasing X and at $X = 0.30$ a minimum value of $\langle A_N \rangle = 15.57$ [G] was reached. At that point in the ternary phase diagram, the isotropic hyperfine coupling constant $\langle A_N \rangle$ indicates that the polarity of the PNIPAM-Py-T precipitate is lower than the cyclic ether THF ($\langle A_N \rangle = 15.65$ [G]) [22]. Note that this precipitate is formed from 4.0 $g \cdot l^{-1}$ polymer in H_2O/MeOH 65:35 (v/v) ($\langle A_N \rangle$ of this solvent mixture: 17.0 [G]). After passing through the minimum, the observed $\langle A_N \rangle$ displays the same function as the hyperfine coupling behavior of PNIPAM-T: the $\langle A_N \rangle$ increases up to at $X = 0.58$, where the two phases become one. Then, the curve follows the $\langle A_N \rangle$ behavior found already in mixtures of both solvents.

The decrease of PNIPAM-T continued until an extremum at $X = 0.442$ ($\langle A_N \rangle = 16.09$) was reached. Note that the experimentally observed hyperfine coupling constants for both PNIPAM-Py-T and PNIPAM-T are lower than found in either solvent and indicate, therefore, the distinctly low polarities of the (labeled) PNIPAM precipitates. This behavior is indicative of an almost complete solvent extrusion during the process of the formation of PNIPAM precipitate [11]. This mechanistic paradigm gained recently experimental support from light-scattering experiments [14].

After passing through the extremum, the $\langle A_N \rangle$ values of PNIPAM-T increases until in the region of $X \approx 0.6$ the observed $\langle A_N \rangle$ merges again with the curves, which were already seen employing 4-amino-TEMPO in H_2O/MeOH in the presence and in the absence of 4.0 $g \cdot l^{-1}$ PNIPAM. In this region of the ternary diagram, the LCST phenomenon disappears, and the phase diagram returns there to a single phase. From this behavior, we were able to conclude that the LCST and the hyperfine coupling of polymer-attached TEMPO are indeed linked phenomena.

The characteristic slope of $\langle A_N \rangle$ of PNIPAM-T cannot be observed, when TEMPO is not chemically attached to the polymer. The reason for this is most likely that the rather hydrophilic spin probe becomes extruded together with the solvent mixture during LCST and is then located in the bulk solvent (and not in the precipitated polymer)!

This finding must be regarded as the key result of this study: whereas PNIPAM, PNIPAM-T, and PNIPAM-Py-T display almost the same LCST behavior in the ternary diagrams formed with H_2O and MeOH as co-nonsolvent, they feature distinctly different physical properties of the formed precipitates. The $\langle A_N \rangle$ analysis reveals a very simple method to design PNIPAM possessing tailor-made hydrophobicities, which can serve as nanoreactors for many applications in the fields of nanotechnology and life sciences.

3. *Photophysical Studies.* The comparison of the experimental results previously obtained by using PNIPAM [10] and PNIPAM-T [12][22] with the (photo)physical properties of PNIPAM-Py-T offers an intriguing opportunity: it was the goal of our work to elucidate, how much the physical properties of (labeled) PNIPAM precipitate are influenced by the presence of the chemically attached pyrene units. It is well-established that PNIPAM-attached pyrene forms in aqueous solution and ternary aqueous mixtures so-called static excimers [23]. The hydrophobicity of pyrene can be regarded as the driving force for the formation of such performed excimers. However, during the process of precipitation of PNIPAM, the amount of preformed excimer decreases significantly because of the hydrophobic interaction between pyrene and the forming PNIPAM precipitate [10][12].

The authors demonstrated previously by employing the spin-labeled copolymer PNIPAM-T, that PNIPAM precipitated from H_2O/MeOH mixtures was distinctly more hydrophobic than dissolved in either H_2O or MeOH [11]. This conclusion was drawn from the measured isotropic hyperfine coupling constants $\langle A_N \rangle$ of TEMPO spin-probes, which were chemically attached to the polymer's backbone.

Furthermore, it could be proved by the same experimental technique that almost all solvent molecules are extruded during the process of PNIPAM precipitation. By using the same experimental approach, the influence of chemically attached pyrene units on the hydrophobicity of the PNIPAM precipitate can be determined. The knowledge of the influence of a chemically attached spin-probe in the physical properties of an investigated (co)polymer is of a special interest.

However, the experimental observation of the influence of the chemically attached TEMPO units on the physical properties cannot be monitored independently by monitoring the fluorescence from the co-attached pyrene units, because TEMPO strongly quenches the fluorescence of pyrene [24]. Therefore, two factors strongly influence the pyrene fluorescence lifetimes as well as the quantum efficiencies of photon emission: *a*) the hydrophobicity of the local environment of pyrene, and *b*) the quenching of the monomer and the excimer fluorescence by TEMPO.

The photophysical behavior of PNIPAM-Py-T in comparison to PNIPAM-Py and (pyren-1-yl)methyl butyrate was discussed in detail in [11]. The fluorescence spectrum of PNIPAM-Py-T in H_2O at $T = 25°$ reveals an emission originating from locally excited Py (intensity I_M, monomer emission) with the (0,0) band located at 378 nm and a second broad featureless emission centered at 480 nm arising from pyrene excimers (intensity I_E). The total emission quantum efficiency of the PNIPAM-Py-T fluorescence in H_2O at $T = 25°$ ($\phi_\tau = 0.45$) was found to be only slightly lower than that of PNIPAM-Py under the same conditions ($\phi_\tau = 0.52$). A detailed analysis of the spectral features of the excimer emission, reported in [12], revealed that it originates from preformed pyrene ground-state aggregates that form prior to excitation. Furthermore, we have determined the quenching constants of PNIPAM-bound pyrene with freely diffusing TEMPO (2,2′,6,6′-tetramethylpiperidine 1-oxide): quenching proceeded diffusion-controlled in H_2O ($k_q = 1.4 \times 10^9$ ($M^{-1} \cdot s^{-1}$ at 25°) and MeOH ($k_q = 8 \times 10^9$ $M^{-1} \cdot s^{-1}$ at 25°).

In *Fig. 6*, the emission quantum efficiencies for the monomer-, excimer-, and total emission from PNIPAM-T-bound pyrene in H_2O/MeOH mixtures are summarized. It becomes clear that rather drastic changes were observed. Starting from ($\phi_\tau = 0.43$),

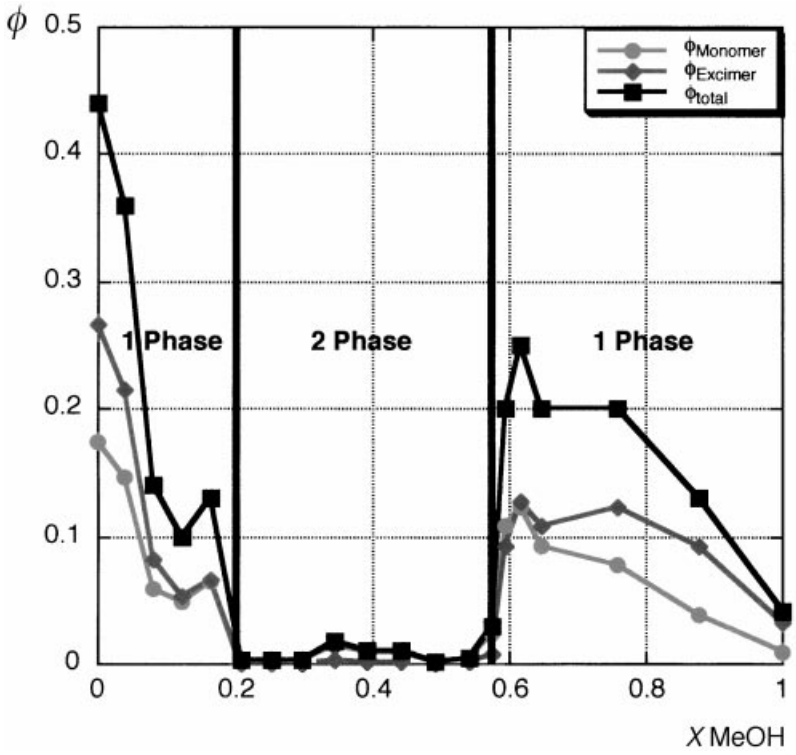

Fig. 6. *Apparent fluorescence quantum efficiencies of PNIPAM-Py-T* (2.0 g; dissolved in mixtures H_2O/MeOH, $T = 20°$)

measured in H_2O at $T = 20°$, the apparent emission quantum efficiencies decreased stepwise upon addition of MeOH. At $X = 0.165$, a total emission efficiency $\phi_\tau = 0.13$ was measured. The observed decrease of ϕ_τ is consistent with the preferential adsorption of MeOH at PNIPAM, which was discovered earlier [11] by EPR spectroscopy. The preferential adsorption of MeOH must be regarded as the first mechanistic step of the collapse process of individual PNIPAM chains, when observed along an isotherm through the ternary phase diagram H_2O/MeOH/PNIPAM. The enrichment of MeOH in the direct proximity of PNIPAM leads to distinctly lower emission quantum efficiencies of chemically attached pyrene ($\phi_\tau = 0.03$ in MeOH at $T = 20°$). The next step in the PNIPAM precipitation consists in the so-called coil-to-globule transition; individual PNIPAM chains collapse and form nanoglobules. According to our EPR results, the solvent molecules become almost completely extruded during this process. The formed nanoglobules scatter the excitation light efficiently, and thus precipitated PNIPAM has a white color (when excited using polychromatic light). This scattering effect leads to the drastic decrease in the observed apparent emission quantum efficiencies. Between $X = 0.21$ and $X = 0.58$, the measured ϕ_τ data ranged from 0.0027 to 0.018 in the two-phase region of the ternary phase diagram. Beyond $X = 0.58$, the phase diagram returns abruptly to one phase. At $X \approx 0.59$, ϕ_τ jumps back to 0.2 and decreases then again step by step upon addition of

MeOH. In this domain of the ternary phase diagram, a preferential adsorption of MeOH at PNIPAM-Py-T cannot be concluded from the data available.

Although the apparent fluorescence quantum efficiencies permit the elucidation of the one-phase *vs.* the two-phase domains following an isotherm at $T = 20°$ through the ternary phase diagram PNIPAM-Py-T/H_2O/MeOH, they permit only a little insight in the molecular interaction between the (precipitated) PNIPAM and the attached (pyrene) labels. Therefore, we plotted the ratio of quantum efficiencies of monomer emission ϕ_M and excimer emission ϕ_E *vs. X* MeOH. The result is shown in *Fig. 7.* The quotient of ϕ_M/ϕ_E is smaller than 1.0 between $X = 0.0$ to < 0.2 and between > 0.60 and 1.0. This finding indicates the prevailing of preformed excimers, when PNIPAM is dissolved in H_2O/MeOH. This mechanism is so effective that the emission from pyrene excimers exceeds that of pyrene monomers. From this finding, we conclude that the presence of pyrene excimers, formed from chemically attached pyrene units in the ground state, leads to the partial cross-linking of individual PNIPAM chains in the 'one-phase domains' of the ternary phase diagram. However, these cross-linking excimers are broken up, when the LCST is reached, because of the superior hydrophobicity of the formed PNIPAM precipitate. The subsequent disappearance of the pyrene-excimer content is indicated by a remarkable increase of the quotient ϕ_M/ϕ_E in the two-phase

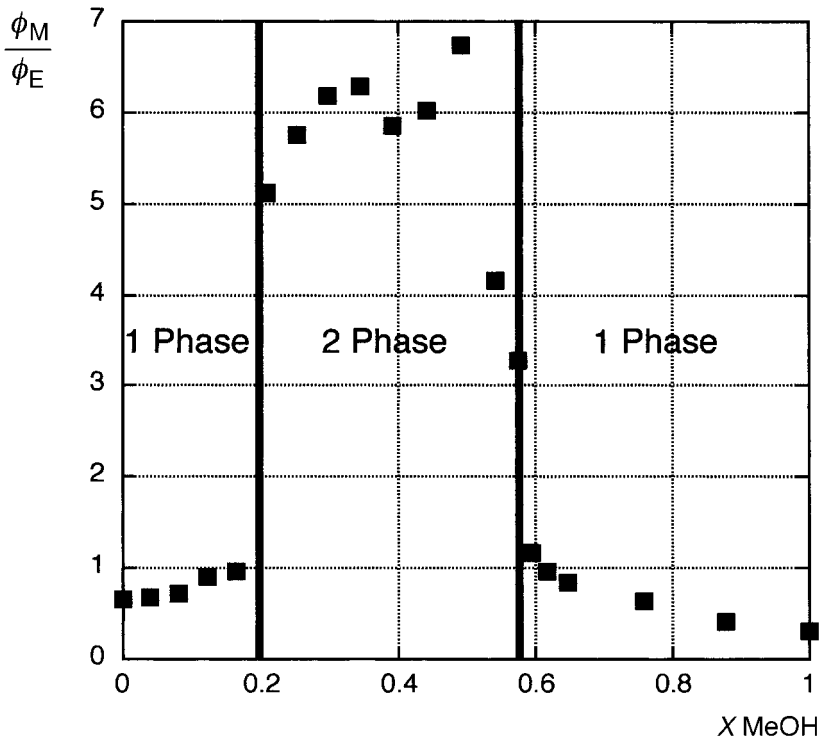

Fig. 7. *Quotient of the quantum efficiencies of monomer emission* ϕ_M *and excimer emission* ϕ_E *plotted* vs. κ *MeOH*

domain, where values up to $\phi_M/\phi_E = 7$ are reached. This finding is principally in agreement with the photophysical behavior of PNIPAM-Py [10]. Furthermore, it can be regarded as further experimental proof that both, the pyrene and the TEMPO labels, are randomly connected to the PNIPAM backbone.

Conclusion. – We have investigated the thermally reversible phase transition of a pyrene- and TEMPO-labeled poly(*N*-isopropylacrylamide) copolymer (PNIPAM-Py-T) by three independent techniques: cloud-point formation, CW-ESR spectroscopy of the chemically attached TEMPO spin-label, and photophysical investigation of the fluorescence arising from the polymer-bound pyrene labels. The analysis of the EPR line-shapes revealed the different motion characteristics of PNIPAM-Py-T in H_2O/MeOH, and THF. In H_2O (below the LCST), the hydrophobic pyrene units are associated within intrapolymeric microdomains, from which the hydrophilic TEMPO spin-labels are almost completely precluded. Furthermore, the associated H_2O layer at PNIPAM-Py-T causes the appearance of two EPR components. When MeOH is added to form a ternary phase diagram, we have obtained evidence for the preferential adsorption of the co-nonsolvent at PNIPAM. Our investigations could confirm that, following an isotherm through the ternary phase diagram, individual macromolecules collapse from extended chains, partially 'cross-linked' by preformed pyrene ground-state aggregates in solution, into nanoglobules. The latter process proceeds under the almost complete extrusion of the solvent mixture. Furthermore, the analysis of the isotropic hyperfine coupling constant revealed that the hydrophobicity of the precipitate formed from PNIPAM-Py-T is significantly enhanced in comparison to that of PNIPAM-T. This finding offers the use of the formed PNIPAM nanoglobules as nanoreactors for application in the fields of nanotechnology and life sciences. They have already been employed successfully for the photo-initiated synthesis of nanoscopic polymer latex particles [3]. Our photophysical experiments, which were concerned with the fluorescence quantum efficiency of pyrene monomer and excimer emission, confirmed the results obtained from EPR spectroscopy.

The authors would like to acknowledge the financial support of this work by the *Industry/University Cooperative Center* at Columbia University, *National Science Foundation* (EEC-9804618), and the industrial sponsors of the IUCR Center. Financial support from *NATO* (CRG 38083) and from the *Deutsche Forschungsgemeinschaft* (BO-1060/III) is also gratefully acknowledged.

REFERENCES

[1] T. A. Smith, J.-I. Hotta, K. Sasaki, H. Masuhara, Y. Itoh, *J. Phys. Chem. B* **1999**, *103*, 1660.
[2] A. Weiss, M. Hartenstein, N. Dingenouts, M. Ballauff, *Colloid Polym. Sci.* **1998**, *276*, 794.
[3] M. R. Pokhrel, K. Janik, S. H. Bossmann, *Macromolecules* **2000**, *33*, 3577.
[4] M. Heskins, J. E. Guillet, *J. Macromol. Sci., Chem*. **1968**, *A2*, 1441.
[5] Y. Maeda, T. Nakamura, I. Ikeda, *Macromolecules* **2001**, *34*, 1391.
[6] A. Percot, X. X. Zhu, M. Lafleur, *J. Polym. Sci.*, *Part B: Polym. Phys.* **2000**, *38*, 907.
[7] J.-M. Guenet, 'Thermoreversible Gelation of Polymers and Biopolymers', Academic Press, San Diego, 1992.
[8] H. G. Schild, D. A. Tirrell, *J. Phys. Chem*. **1990**, *94*, 4352.
[9] K. Kubota, S. Fujishige, I. Ando, *J. Phys. Chem*. **1990**, *94*, 5154.
[10] F. M. Winnik, *Macromolecules* **1990**, *23*, 233.
[11] F. M. Winnik, M. F. Ottaviani, S. H. Bossmann, W. Pan, M. Garcia-Garibay, N. J. Turro, *J. Phys. Chem*. **1993**, *97*, 12998.

[12] F. M. Winnik, M. F. Ottaviani, S. H. Bossmann, M. Garcia-Garibay, N. J. Turro, *Macromolecules* **1992**, *25*, 6007.
[13] D. Duracher, F. Sauzedde, A. Elaissari, A. Perrin, C. Pichot, *Colloid Polym. Sci*. **1998**, *276*, 219.
[14] G. Zhang, C. Wu, *J. Am. Chem. Soc*. **2001**, *124*, 1376.
[15] F. M. Winnik, *Macromolecules* **1987**, *20*, 2745.
[16] S. Fujishige, *Polym. J.* **1987**, *19*, 297.
[17] D. J. Schneider, J. H. Freed, in 'Biological Magnetic Resonance', Ed. L. J. Berliner, J. Teuben, Plenum Press, New York, 1989, Vol. 8, p. 1 – 76.
[18] N. J. Turro, 'Modern Molecular Photochemistry', The Benjamin/Cummings Publishing Co., Menlo Park, A, 1978, p. 117.
[19] A. N. Fletcher, *Photochem. Photobiol*. **1969**, *9*, 439.
[20] K. A. Sharp, E. M. Bhupinder, J. M. Vanderkooi, *J. Chem. Phys.* **2001**, *114*, 1791.
[21] M. A. M. Noel, R. D. Allendoerfer, R. A. Osteryoung, *J. Phys. Chem*. **1992**, *96*, 2391.
[22] F. M. Winnik, M. F. Ottaviani, S. H. Bossmann, W. Pan, M. Garcia-Garibay, N. J. Turro, *Macromolecules* **1993**, *26*, 4577.
[23] F. M. Winnik, *Chem. Rev.* **1993**, *93*, 587.
[24] M. V. Encinas, E. A. Lissi, J. Alvarez, *Photochem. Photobiol*. **1994**, *59*, 30.

Received May 19, 2001